**Geomechanics and Engineering**, *Vol. 39, No. 5 (2024) 475-482*
https://doi.org/10.12989/gae.2024.39.5.475


# Development and experimental validation of P-Y curves for rectangular piles

Wenshuai Li[a], Weiming Gong* and Guoliang Dai[b]

*School of Civil Engineering, Southeast University, Nanjing 211189, China*

(*Received April 1, 2024, Revised November 21, 2022, Accepted November 27, 2024*)

**Abstract.** This paper conducted in-situ horizontal load tests on rectangular piles both before and after grouting and systematically analyzed the data. Firstly, the typical response characteristics of rectangular piles in gravelly soil under horizontal loading were determined. Secondly, a set of *p-y* curve models applicable to rectangular section piles was constructed by utilizing hyperbolic equations combined with the in-situ shear strength parameters and deformation parameters of the soil. Finally, based on the constructed *p-y* curve models, various important factors determining the response of rectangular piles under horizontal loading were analyzed in detail.

**Keywords:** field test; gravelly soil; *p-y* curves; rectangular pile; ultimate lateral resistance

## 1. Introduction

Rectangular section piles are widely utilized in large-scale structural foundations worldwide due to their excellent performance (Manoj *et al*. 2022, Laveti *et al*. 2024, Nguyen *et al.* 2024). They can withstand immense horizontal and vertical loads, and their rectangular shape minimizes disturbance to the surrounding environment, requiring minimal excavation, thus making them adaptable to various construction scenarios (Ramaswamy and Pertusier 1986, Lei 2001). Rectangular section piles have a larger surface area compared to circular piles, resulting in broader contact with the soil, thereby more effectively mobilizing the lateral frictional resistance between the pile and soil. This larger contact area gives rectangular section piles an advantage in terms of energy exchange compared to traditional circular piles, making them widely used in the field of energy piles (Loria *et al.* 2022, 2023). Additionally, due to the asymmetry of the rectangular section, it can be flexibly arranged according to the layout of the foundation to maximize its bending stiffness, providing more stable support for the structure (Align *et al.* 2022). The analysis results suggest that, in comparison to circular piles with equal cross-sectional area, barrettes demonstrate a higher bearing capacity. Furthermore, the bearing capacity along the major axis direction for barrettes with an equal cross-sectional area surpasses that of circular piles (Behloul *et al.* 2023).

Experimental research indicates a close correlation between the load response of rectangular section horizontal piles and the loading direction. Due to the asymmetry of the pile section, rectangular piles exhibit significant differences in load-bearing capacity when subjected to horizontal loads along the major and minor axes. The load-carrying capacity under horizontal loads decreases gradually with the increasing angle between the loading direction and the major axis of the section. The horizontal load-carrying capacity of rectangular piles reaches its minimum when the loading direction coincides completely with the minor axis of the section (Zhang 2003, Wakil and Nazir 2013). Under horizontal loading, the resistance generated by the interaction between the pile and soil mainly consists of soil resistance ahead of the pile and lateral soil resistance. The dominant component is the soil resistance ahead of the pile, while the contribution of lateral frictional resistance to the total resistance is relatively low (Wang 2021, 2023, Smith 1987).

Based on a comprehensive analysis of experimental data from in-situ horizontally loaded piles, Janoyan and Whelan (2004) revealed the distribution pattern and mechanism of soil resistance around the piles. The results indicate that the influence of active earth pressure behind the pile on the calculation of total soil resistance can be almost negligible. At small pile deflections, lateral soil resistance is mobilized, and as the pile deformation increases, the proportion of soil resistance ahead of the pile in the total soil resistance gradually increases. However, this change does not strictly correlate with the increase in pile deflection. Building on the actual stress distribution of soil around the pile, Jiang *et al.* (2022) analyzed the horizontal load characteristics of piles in sand using the *p-y* curve method and concluded that the lateral soil resistance accounts for only about 10% of the total resistance.

After systematically analyzing the load characteristics of numerous horizontally loaded piles, Reese and Van Impe (2000) indicated that the soil resistance generated by pile-soil interaction is influenced by the shape of the pile section.

Zhou *et al.* (2014) analyzed the interaction phenomenon between piles and soils of horizontally loaded section piles in elastoplastic media. Under the conditions of horizontal

*Corresponding author, Professor
E-mail: wmgong@seu.edu.cn
[a]Ph.D. Student
[b]Professor



ISSN: 2005-307X (Print), 2092-6219 (Online)

loading, a passive earth pressure zone is formed in the front part of rectangular section piles. With the increase in load, the soil surrounding the pile will exhibit an approximately rectangular plastic deformation profile. Stress concentration phenomena occur at the corners of the rectangular section. Ukritchon and Keawsawasvong (2018) found a direct correlation between the range and morphological dimensions of pile-soil interaction and the adhesive coefficient between the pile and the soil. Square piles with rough cross-sections typically exhibit arc-shaped features on their sliding shear surfaces under loading. Adeel *et al.* (2022) conducted numerical simulations and analyses to study the lateral load response of pile foundations in granular soils, assessing the reliability of using empirical *p-y* curves for beams in the nonlinear Winkler foundation model. They recommended further research to refine p-y curves and p-multipliers for granular soils to enhance pile foundation design under lateral loading conditions.

This paper analyzes the load response of horizontally loaded rectangular piles before and after grouting, constructing a *p-y* curve model suitable for rectangular section piles by utilizing hyperbolic equations along with the in-situ shear strength parameters and deformation parameters of the soil. Furthermore, based on the constructed *p-y* curves, this paper conducts an analysis of the factors influencing the response of rectangular piles under horizontal loading.

## 2. Site and soil characterization

As shown in Fig. 1(a), the experimental site is located on the slope of the Jinsha River in Kahaluo Township, Sichuan Province, China. The slope is covered with an exceptionally thick layer of overburden. The geological survey drilling shows that the stratum where the experimental pile is located mainly consists of Upper Pleistocene collapse slope alluvium, characterized by block stones, gravel, and breccia. The stone composition is mainly strong to medium-weathered mudstone. The deep collapse body experiences minimal weathering and subsequent geological movements, resulting in the formation of block stones. Conversely, the upper to middle portion is significantly affected by weathering and geological movements, causing the bedrock collapse body to degrade into gravel. The breccia mainly originates from interlayer fracture zones within the collapsed body. The typical geological borehole profile is depicted in Fig. 1(b).

The undisturbed samples of gravelly soil exhibit structural complexity, making it challenging to reliably determine physical-mechanical parameters through laboratory experiments. Therefore, an adit was excavated on-site to conduct in-situ geotechnical tests on the gravelly soil. The adit is approximately 25 m long, about 2.0 m wide, and roughly 2 m high. Inside the adit, the rock soil is dense and exhibits good cementation. As depicted in Fig. 2, following Chinese standard DL/T 5356-2006, full-scale direct shear tests and lateral plate load tests were conducted.

The specimens for the direct shear test have uniform dimensions, with lengths and widths both measuring 0.9 m

(a) Site characteristics

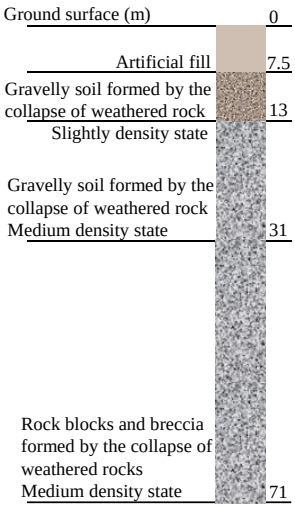


(b) Subsurface profile of the test site

Fig. 1 test site characteristics

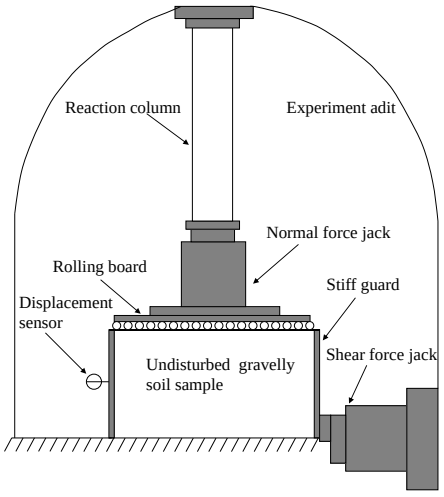


(a) Full-scale direct shear test

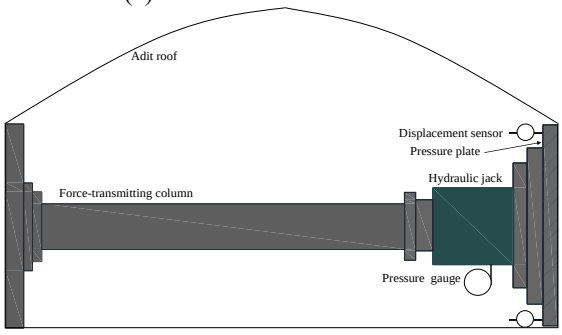


(b) lateral plate load test

Fig. 2 Geotechnical parameter testing

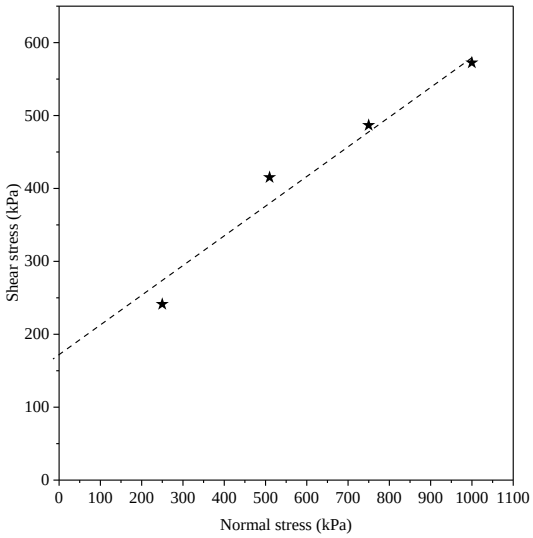


(a) Shear strength envelope

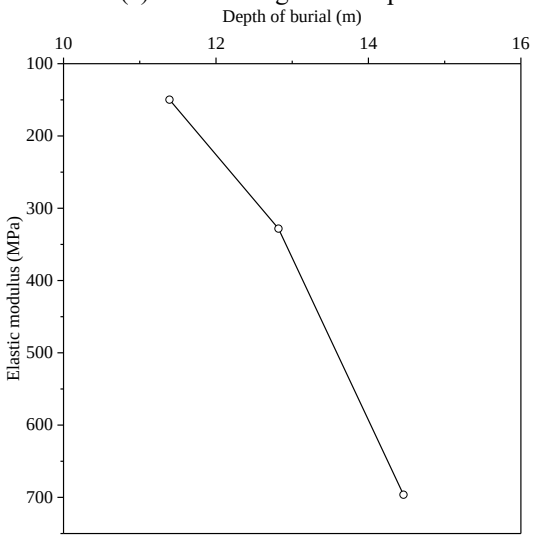


(b) Elastic modulus

Fig. 3 Geotechnical parameters

and a height of 0.5 m. The test consists of 2 groups, each containing 4 independent test points, totaling 8 test points. Moreover, lateral plate load tests were conducted at three different burial depths, with five cycles of loading and unloading performed at each location. The modulus of elasticity for the geotechnical material, $E_s$, was derived using the principles of elastic theory.

The shear strength envelope of gravel soil, as depicted in Fig. 3(a), exhibits a cohesive strength of 128 kPa and an internal friction angle of 26°. The soil average elastic modulus $E_s$ is 595 MPa, with a united weight $\gamma$ of 24 kN/m$^3$. The relationship between the elastic modulus of soil and burial depth is shown in Fig. 3(b).

## 3. Experiment details and results

The reinforcement cage of the experimental pile has longitudinal steel bars with a diameter of 32 mm and a yield strength of 400 MPa. Rigid concrete blocks are used to

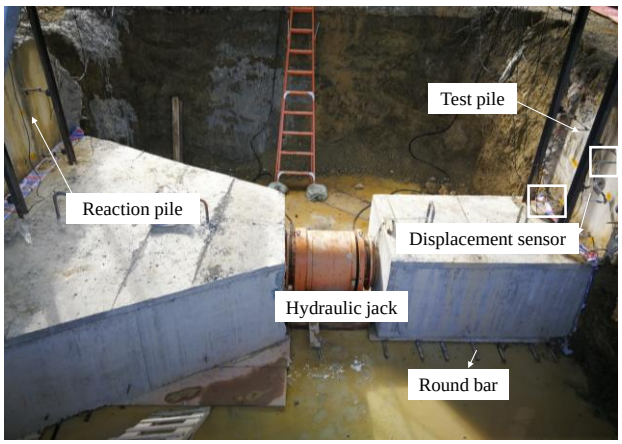


(a) Experimental setup

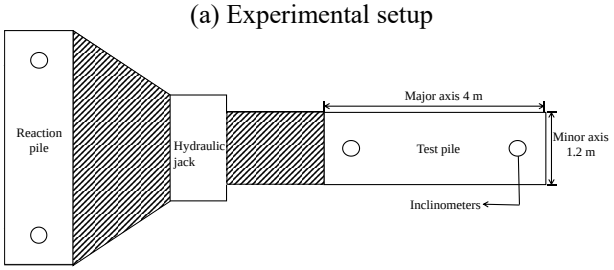


(b) Plan layout

Fig. 4 Static lateral load test on rectangular piles

transmit loads between the experimental pile and the reaction pile. Circular steel bars are positioned under the concrete block to reduce friction. Loading is accomplished using horizontal hydraulic jacks.

The experiment was conducted using the slow load maintenance method specified in Chinese standard JTG/T 3512-2020. The experiment is divided into before grouting and after grouting phases. Before grouting, a maximum load of 7 MN is applied, which increases to 10 MN post-grouting. Inclinometers attached to the steel reinforcement cage are used to measure the pile's deflection. Inclinometers have been affixed to the reinforcement cage for measuring the deflection of the pile, while displacement sensors have been positioned at the pile head to monitor changes in displacement, as illustrated in Fig. 4.

The experimental pile, 25 m in length, has a cross-sectional major axis of 4 m and a minor axis of 1.2 m. The major axis moment of inertia is 7.1 m$^4$, and the Stiffness ratio between pile and soil $K_R$ is $9.1\times10^{-4}$. According to the relative stiffness criterion, it is classified as a flexible pile (Poulos and Davis 1980).

As shown in Fig. 5, the load-displacement curve displays nonlinearity at small displacements, with the initial slope after grouting greater than that before grouting. With increasing load, the slope of the load-displacement curve gradually decreases, indicating a reduction in the load required to generate a unit displacement.

As depicted in Fig. 6, the deflection of the pile gradually diminishes with increasing depth, reaches zero deflection at the base of the pile. Before grouting, the depth of zero deflection of the pile is approximately 8.3 times the minor axis length, while after grouting, this depth increases to about 10.8 times the minor axis length. With increasing

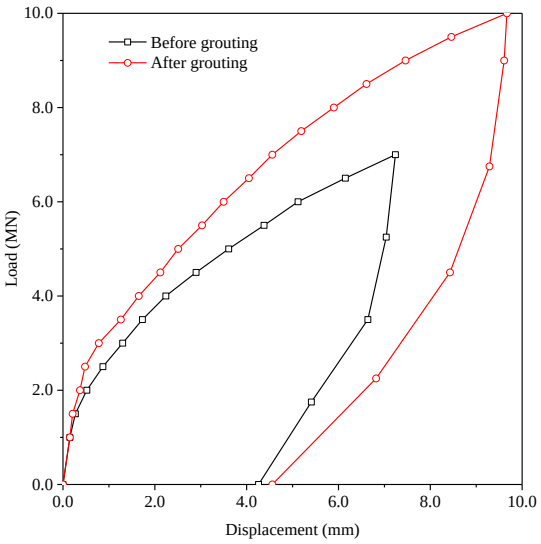


Fig. 5 Load-displacement relationship

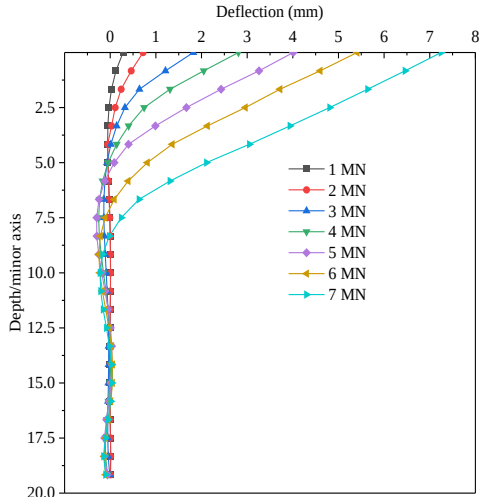


(a) Before grouting

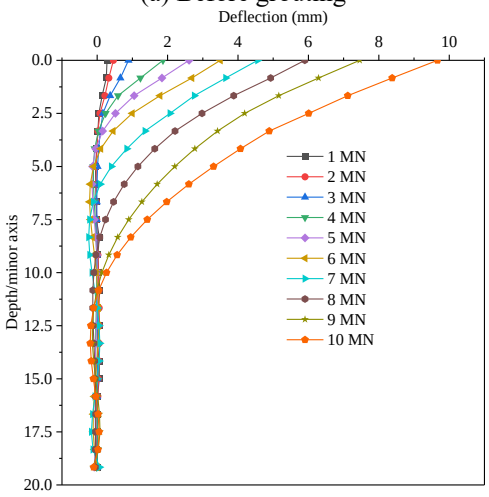


(b) After grouting

Fig. 6 Deflection-depth relationship

load, the zero deflection point gradually shifts downwards, indicating the deformation characteristics of a semi-rigid pile.

## 4. Discussion

### *4.1 P-y response*

With the exception of short piles, the soil resistance primarily consists of the normal stress at the pile front and the shear stress at the pile side (Briaud *et al.* 1984). Based on the variation pattern of pile-soil relative stiffness and pile deflection, it can be inferred that the test pile exhibits characteristics of a semi-rigid pile under loading. Consequently, the *p-y* curves method can be adopted to evaluate the pile's load response.

The hyperbolic equation-derived *p-y* curve is widely utilized in a variety of geological materials, including clay (Georgiadis and Georgiadis 2012), sand (Zhu *et al.* 2016), weathered soil (Jeong *et al*. 2017 ), soil-rock mixtures (Yu *et al.* 2018) and rocks (Liang *et al.* 2009, Elsokary *et al.* 2023). This demonstrates the broad applicability of the hyperbolic equation to both soil and rocks. Therefore, in this study, the hyperbolic function is utilized to characterize the *p-y* relationship of gravelly soil.

$$P = \frac{y}{\frac{1}{k_h} + \frac{y}{p_{ult}}} \tag{1}$$

Where $k_h$ represents subgrade modulus, $p_{ult}$ denotes ultimate soil resistance per unit length, $y$ signifies pile deformation.

### *4.2 Initial stiffness*

Fransic (1964) builds upon the studies conducted by Biot (1937) and Vesić (1961) on beams supported by a semi-infinite elastic foundation, applying it to the analysis of piles. Fransic (1964) proposes that the initial stiffness $k_h$ in *c-φ* soil can be calculated by Eq. (2). Moreover, Georgiadis. and Georgiadis (2012) demonstrated that Eq. (2) provides a reasonably accurate estimation of the initial stiffness in *c-φ* soil, with discrepancies not exceeding 15%.

$$k_h = 1.3\frac{E_s}{1-\mu^2}\left(\frac{E_s b^4}{E_p I_p}\right)^{\frac{1}{12}} \tag{2}$$

Here, $\mu$ denotes the Poisson's ratio of the soil, with a specified value of 0.27 according to the Chinese standard GB 50021-2001. $E_s$ represents the elastic modulus of the soil, $b$ denotes the minor axis of the pile section, $E_p$ indicates the elastic modulus of the pile, and $I_p$ represents the moment of inertia of the pile.

Terzaghi (1955) proposed the hypothesis that the subgrade modulus $k_h$ of granular soils increases proportionally with depth. Although the actual variation of subgrade modulus with depth is not strictly linear, the linear incremental description of subgrade modulus variation is the most practical for theoretical applications (Prakash 1962). The average value of subgrade modulus $k_h$, calculated using Eq. (3), is determined to be 539 MN/m$^2$ based on the elastic modulus deriving from the field test. The relationship between $k_h$ and depth $z$ can be established using Eq. (3).

$$k_h = 43.8z + 539 \tag{3}$$

Here $z$ is depth.

### *4.3 Ultimate resistance*

During horizontal movement of the pile, the soil resistance it experiences consists of two components: normal and tangential components on the surface (Simth 1987, Carter and Kulhawy 1992). This has been confirmed by experiments or theoretical analysis (Wang *et al.* 2023, Janoyan and Whelan 2004, Jiang *et al.* 2022). Drawing from the investigation into the distribution of pile side stress for horizontally loaded piles (Briaud *et al.* 1984), the procedure for calculating ultimate soil resistance is described in Eq. (4).

$$P_{ult} = \xi \tau_{max} l + \eta p_{max} b \tag{4}$$

Here, $\tau_{\max}$ denotes the maximum shear stress at the lateral pile side, $p_{\max}$ is the maximum normal stress at the pile front. $l$ and $b$ represent the lengths of the major and minor axes, respectively. $\eta$ and $\xi$ are shape factors for the stress distributions at the pile front and along the pile side, respectively. Based on the analyses of stress distribution in the soil around the pile by Briaud *et al*. (1984) and Smith *et al.* (1986), the values of $\eta$ and $\xi$ have been determined, as shown in Table 1.

Smith *et al*. (1986) employed pile torsion tests to validate the applicability of Eq. (5) in shear stress calculations, a method later used by Zhang *et al*. (2005) for calculating shear stress in pile-soil interaction.

$$\tau_{max} = K\gamma z \tan\delta \tag{5}$$

$K$ represents the horizontal pressure coefficient; $\delta$ is the friction angle of pile-soil interaction; $\gamma$ is the unit weight of soil; $z$ is depth.

Choi *et al.* (2013) argue that disregarding the cohesive strength of granular soils may underestimate soil resistance. The maximum normal stress $p_{max}$ in undisturbed gravel soil consists of both cementation-cohesive and fractional components (Guo and Lehane 2016).

The undisturbed gravelly soil is classified as $c$-$\varphi$ soil based on the results of full-scale direct shear tests. Considering the influence of cohesion parameter $c$ on maximum normal stress $p_{max}$, a modification to $p_{max}$ is performed using the method proposed by Broms (1964), as specified in Eq. (6).

$$p_{max} = 3(K_p\gamma z + 2c\sqrt{K_p}) \tag{6}$$

$K_p$ is the Rankine passive earth pressure coefficient; $c$ is cohesion.

Before grouting, the influence of mud cake on the pile-soil interface is quantified by parameters $\delta$ and $K$, with values derived from the investigation conducted by Kulhawy *et al*. (1991) on the pile-soil interface of drilled shafts grouted with mud cake, as shown in Table 1. After grouting, effective bond is formed between the pile and the soil, with the values of $\delta$ and $K$ determined based on the soil's strength characteristics, as shown in Table 1.

Table 1 Pile-soil resistance parameters

| condition | parameter | | | |
|---|---|---|---|---|
| | $\delta$ | $K$ | $\xi$ | $\eta$ |
| Before grouting | $0.6\varphi$ | $0.6K_0$ | 1 | 1 |
| After grouting | $\varphi$ | $K_0$ | | |

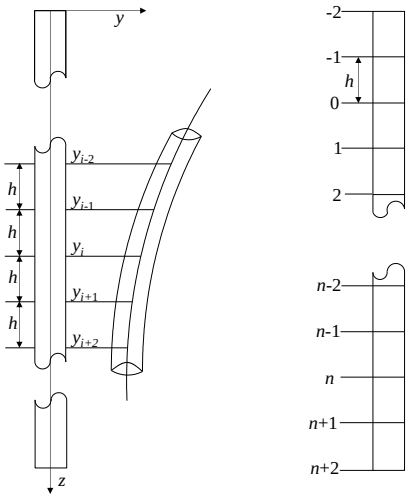


Fig. 7 Finite difference computational model

Where $K_0$ is the coefficient of earth pressure at rest, given by Eq. (7).

$$K_0 = \frac{\mu}{1-\mu} \tag{7}$$

Ultimate soil resistance of gravelly soil before grouting

$$P_{ult} = 3\eta(K_p\gamma z + 2c\sqrt{K_p})b + 1.2\xi K_0 z \tan(0.6\varphi)l \tag{8}$$

Ultimate soil resistance of gravelly soil after grouting

$$P_{ult} = 3\eta(K_p\gamma z + 2c\sqrt{K_p})b + 2(\xi K_0 z \tan\varphi l + c)l \tag{9}$$

### *4.4 Prediction of pile response to load*

The deflection governing equation for laterally loaded piles is presented as Eq. (10).

$$E_p I_p \frac{d^4 y}{dz^4} + P(z) = 0 \tag{10a}$$

$P(z)$ = Soil resistance, determined by the constructed $p$-$y$ curve.

Eq. (10) can be solved through the finite difference method. The pile is discretized into $n$ segments, each with a length of $h$, as shown in Fig. (7)

The finite difference equation at an arbitrary node is

$$(y_{i-2} - 4y_{i-1} + 6y_i - 4y_{i+1} + y_2) + \frac{h^4 P(z)}{E_p I_p} = 0 \tag{10b}$$

Boundary conditions at the pile top

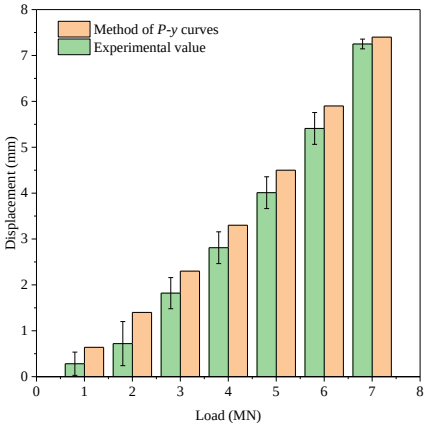


(a) Before grouting

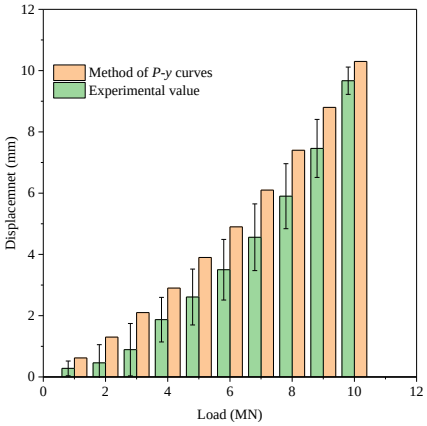


(b) After grouting

Fig. 8 Error between predicted and experimental values

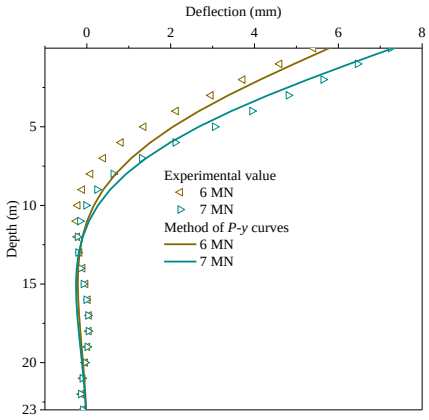


(a) Before grouting

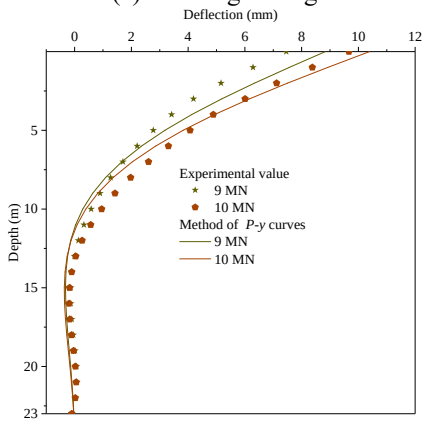


(b) After grouting

Fig. 9 Predicted pile deflection

$$\begin{cases} y_2 - 2y_1 + 2y_{-1} - y_{-2} = \dfrac{2Qh^3}{E_p I_p} \\ y_1 - 2y_0 + y_{-1} = \dfrac{M_0 h^2}{E_p I_p} \end{cases} \tag{11}$$

Boundary conditions at the pile bottom

$$\begin{cases} y_n = 0 \\ y_{n+1} - y_{n-1} = 0 \end{cases} \tag{12}$$

For each node along the pile shaft, a linear equation can be established. Combined with the top and bottom boundary conditions, this results in $n$+5 linear equations. The equation system can be solved using an iterative method.

As depicted in Fig. 8, the pile deflection determined by the *p-y* curves method slightly exceeds the experimental measurement. The variation of error bars indicates that with increasing horizontal load, the error between calculated and measured values gradually decreases. Because the construction parameters of the *p-y* curves are determined based on the mechanical properties of undisturbed gravelly soil, the error between calculated and measured values is relatively small before grouting. However, the grouting process improves the bonding condition between the pile and the soil, thereby influencing the soil and resulting in a greater discrepancy between calculated and measured values after grouting.

As illustrated in Fig. 9, the pile deformation curve predicted by the *p-y* curve method closely matches the measured values, which fully demonstrates the high accuracy of the hyperbolic *p-y* curves constructed based on the shear strength parameters and elastic modulus of the undisturbed gravelly soil in assessing the load characteristics of rectangular piles under horizontal loading.

An analysis of the effect of pile side friction and soil cohesion on the load-displacement curve of rectangular piles is conducted through the *p-y* curves method. As depicted in Fig. 10(a), before grouting, whether considering pile side friction or not, the computed results are relatively close. This indicates that, before grouting, the influence of pile side friction on the load response of rectangular piles is relatively small, and its effect on the load-displacement curve is not significant. However, whether the cohesion of soil is considered has a significant impact on the calculation results. It shows that the cohesion of soil is a crucial factor that cannot be ignored when calculating soil resistance.

Illustrated in Fig. 10(b), after grouting, the influence of pile side friction on the deflection calculation error significantly increases compared to before grouting. This indicates that grouting on the pile side significantly alters the bonding state of the pile and soil, making the influence of pile side friction on the load-displacement curve more pronounced. Meanwhile, the influence of soil cohesion on load response remains significant and similar to the situation before grouting.

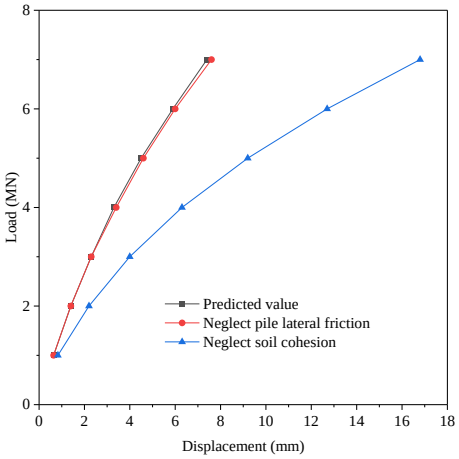


(a) Before grouting

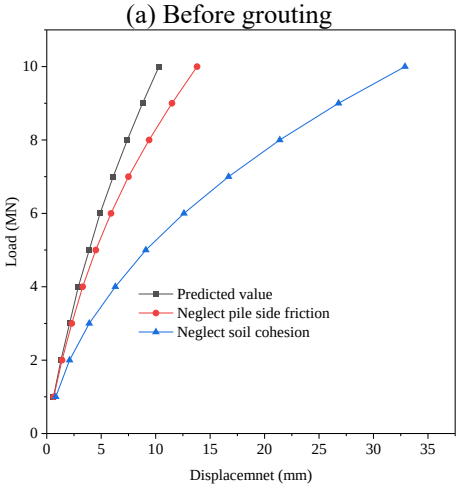


(b) After grouting

Fig. 10 Influence of pile side resistance and soil cohesion on load displacement

## 5. Conclusions

Following the analysis of horizontal load tests on rectangular piles using the *p-y* curve method, the following conclusions were drawn:

• At small displacements, the load-displacement curve of rectangular section piles exhibits significant non-linear characteristics. The combined grouting technique at the pile side and pile tip can effectively reduce the pile head displacement of rectangular piles under the same load, thus enhancing their load-bearing capacity.

• The *p-y* curve constructed based on hyperbolic equations combined with the shear strength parameters and elastic modulus of the soil can accurately predict the response of rectangular piles under horizontal loading, thus providing a reliable basis for engineering practice.

• The larger surface area of rectangular piles results in a more extensive contact area between the pile and soil. Therefore, grouting at the pile sides can significantly enhance the influence of lateral resistance on the pile deflection response, effectively improving the load-bearing capacity and stability of the piles.

• The cohesion of gravelly soil has a significant impact on the load response of pile deflection. Neglecting this key factor of cohesion would underestimate soil resistance, leading to an overestimation of pile deflection prediction values, which introduces significant deviation from actual engineering conditions. Therefore, when analyzing and predicting pile deflection, it is essential to fully consider the cohesive properties of gravelly soil to ensure the accuracy and reliability of the results.

## Acknowledgments

The authors express their gratitude for the funding provided by the National Natural Science Foundation of China (Professors Gong Weiming and Dai Guoliang received support under project numbers, 52178317, and 52378328). Additionally, appreciation is extended for the assistance and cooperation from all employees of Branch Line Two Project Department, Bridge Division, Sichuan Transportation Construction Group Co., Ltd., during the experimental implementation.

## References

Adeel, M.B., Aaqib, M., Pervaiz, U., Rehman, J.U. and Park, D. (2022), "Numerical response of pile foundations in granular soils subjected to lateral load", *Geomech. Eng.*, **28**(1), 11-23. https://doi.org/10.12989/gae.2021.28.1.011.

Algin, H.M., Ekmen, A.B. and Kaya, E. (2022), "3D seismic response assessment of barrette piled high-rise building with comprehensive subsurface modelling", *Soil Dyn. Earthq. Eng.*, **163**, 107488, 1-18 https://doi.org/10.1016/j.soildyn.2022.107488.

Behloul, D., Rafa, S.A. and Moussai, B. (2023), "Numerical analysis of laterally loaded barrette foundation", *Soils Rocks*, **46**(1), 1-8. https://doi.org/10.28927/SR.2023.002122.

Biot, M.A. (1937), "Bending of an infinite beam on an elastic foundation", *J. Appl. Mech.*, **4**(1), 1-7. https://doi.org/10.1115/1.4008739.

Briaud, J.L., Smith, T. and Meyer, B. (1984), "Laterally loaded piles and the pressuremeter: comparison of existing methods", *Laterally loaded deep foundations: Analysis and performance*, Kansas, USA, June. https://doi.org/10.1520/STP36815S.

Broms, B.B. (1964), "Lateral resistance of piles in cohesionless soils", *J. Soil Mech Found. Division*, **90**(3), 123-156. https://doi.org/10.1061/JSFEAQ.0000614.

Carter, J.P. and Kulhawy, F.H. (1992), "Analysis of laterally loaded shafts in rock", *J. Geotech. Eng.*, **118**(6), 839-855. https://doi.org/10.1061/(ASCE)0733-9410(1992)118:6(839).

Choi, H.Y., Lee, S.R., Park, H.I. and Kim, D.H. (2013), "Evaluation of lateral load capacity of bored piles in weathered granite soil", *J. Geotech. Geoenviron. Eng.*, **139**(9), 1477-1489. https://doi.org/10.1061/(ASCE)GT.1943-5606.0000831.

El Wakil, A.Z. and Nazir, A.K. (2013), "Behavior of laterally loaded small scale barrettes in the sand", *Ain Shams Eng. J.*, **4**(3), 343-350. https://doi.org/10.1016/j.asej.2012.10.011.

Elsokary, H.H., El-Sakhawy, N.R., Mahdi, H.A. and Nabil, M. (2023), "A hyperbolic p-y criterion for flexible piles in weathered rock mass", *Int. J. Geomech.*, **23**(10), 04023179, 1-13. https://doi.org/10.1061/IJGNAI.GMENG-8464.

Francis, A.J. (1964), "Analysis of pile groups with flexural resistance", *J. Soil Mech. Found. Division*, **90**(3), 1-32.

https://doi.org/10.1061/JSFEAQ.0000615.
Georgiadis, K. and Georgiadis, M. (2012), "Development of p-y curves for undrained response of piles near slopes", *Comput. Geotech.*, **40**, 53-61. https://doi.org/10.1016/j.compgeo.2011.09.005.
Guo, F. and Lehane, B.M. (2016), "Lateral response of piles in weak calcareous sandstone", *Can. Geotech. J.*, **53**(9), 1424-1434. https://doi.org/10.1139/cgj-2015-0600.
Janoyan, K.D. and Whelan, M.J. (2004), "Interface stresses between soil and large diameter drilled shaft under lateral loading", *Proceedings of the GeoSupport Conference 2004: Drilled Shafts, Micropiling, Deep Mixing, Remedial Methods, and Specialty Foundation Systems*, Orlando, Florida, United States, December. https://doi.org/10.1061/40713(2004)49.
Jeong, S., Park, J., Ko, J. and Kim, B. (2017), "Analysis of soil resistance on drilled shafts using proposed cyclic p-y curves in weathered soil", *Geomech. Eng.*, **12**(3), 505-522. https://doi.org/10.12989/gae.2017.12.3.505.
Jiang, J., Fu, C.Z., Wang, S.W., Chen, C.Q. and Ou, X.D. (2022), "An analytical p-y curve method based on compressive soil pressure model in sand soil", *J. Central South Univ.*, **29**(6), 1987-2004. https://doi.org/10.1007/s11771-022-5044-3.
Kulhawy, F.H. (1991), *Drilled shaft foundations*, In: Foundation Engineering Handbook, Springer US. https://doi.org/10.1007/978-1-4615-3928-5_14.
Laveti, S., Chen, Y.J., Phoon, K.K. and Topacio, A. (2024), "Evaluation of model factors for barrette piles based on cycu/barrette/64", *ASCE-ASME J. Risk Uncertainty in Eng. Syst.*, *Part A: Civil Eng.*, **10**(1), 04023056, 1-25. https://doi.org/10.1061/AJRUA6.RUENG-1147.
Lei, G. (2001), "Behaviour of excavated rectangular piles (barrettes) in granitic saprolites", Hong Kong University of Science and Technology, Hong Kong, China.
Liang, R., Yang, K. and Nusairat, J. (2009), "P-y criterion for rock mass", *J. Geotech. Geoenviron. Eng.*, **135**(1), 26-36. https://doi.org/10.1061/(ASCE)1090-0241(2009)135:1(26).
Loria, A.F.R., Ravera, E. and Laloui, L. (2023), "Thermo-hydro-mechanical behavior of energy barrettes: Field experiments and numerical simulations", *Geomech. Energ. Environ.*, **34**, 100451, 1-13. https://doi.org/10.1016/j.gete.2023.100451.
Loria, A.F.R., Richard, N. and Laloui, L. (2022), "Analysis of barrette foundations subjected to mechanical and thermal loads", *Geomech. Energ. Environment*, **32**, 100333, 1-14. https://doi.org/10.1016/j.gete.2022.100333.
Manoj, S., Choudhury, D. and Alzaylaie, M. (2022), "Value engineering using load-cell test data of barrette foundations-La Maison, Dubai", *Proceedings of the Institution of Civil Engineers-Geotechnical Engineering*, **175**(3), 340-352. https://doi.org/10.1680/jgeen.19.00246.
Nguyen, T. and Fellenius, B.H. (2024), "Bidirectional static loading tests on barrette piles", A case history from Ho Chi Minh City, Vietnam", *Can. Geotech. J.*, e-First. https://doi.org/10.1139/cgj-2023-0098.
Poulos, H.G. and Davis, E.H. (1980), *Pile Foundation Analysis And Design*, Wiley, New York, USA.
Prakash, S. (1962), "Behavior of pile groups subjected to lateral loads", Ph.D. Dissertation, University of Illinois, Urbana-Champaign, Illinois, USA.
Ramaswamy, S.D. and Pertusier, E.M. (1986), "Construction of barrettes for high-rise foundations", *J. Constr. Eng. Management*, **112**(4), 455-462. https://doi.org/10.1061/(ASCE)0733-9364(1986)112:4(455).
Reese, L.C. and Van Impe, W.F. (2000), *Single piles and pile groups under lateral loading* (2nd Ed.), CRC Press, London. https://doi.org/10.1201/b17499.
Smith, T. and Slyh, R. (1986), "Side friction mobilization rates for laterally loaded piles from the pressuremeter", *Proceedings of the Pressure-meter and Its Marine Applications: 2nd International Symposium,* Texas, U.S, May. https://doi.org/10.1520/STP19302S.
Smith, T.D. (1987), "Pile horizontal soil modulus values", *J. Geotech. Eng.*, **113**(9), 1040-1044. https://doi.org/10.1061/(ASCE)0733-9410(1987)113:9(1040).
Smith, T.D. (1987), "Pile horizontal soil modulus values", *J. Geotech. Eng.*, **113**(9), 1040-1044. https://doi.org/10.1061/(ASCE)0733-9410(1987)113:9(1040).
Terzaghi, K. (1955), "Evaluation of coefficients of subgrade reaction", *Geotechnique*, **5**(4), 297-326. https://doi.org/10.1680/geot.1955.5.4.297.
Ukritchon, B. and Keawsawasvong, S. (2018), "Undrained lateral capacity of rectangular piles under a general loading direction and full flow mechanism", *KSCE J. Civil Eng.*, **22**(7), 2256-2265. https://doi.org/10.1007/s12205-017-0062-7.
Vesić, A.B. (1961), "Bending of beams resting on isotropic elastic solid", *J. Eng. Mech. Division*, **87**(2), 35-53. https://doi.org/10.1061/JMCEA3.0000212.
Wang, C., Liu, H., Ding, X., Wang, C. and Ou, Q. (2021), "Study on horizontal bearing characteristics of pile foundations in coral sand", *Can. Geotech. J.*, **58**(12), 1928-1942. https://doi.org/10.1139/cgj-2020-0623.
Wang, C., Liu, J., Chen, Z., Jiang, C. and Ding, X. (2023), "A modified p–y model of single pile in coral sand under lateral load", *Can. Geotech. J.*, **60**(3), 334-350. https://doi.org/10.1139/cgj-2021-0314.
Yu, Y., Sun, H. and Juang, C.H. (2018), "A new model for response of laterally loaded piles in soil-rock mixtures", *Comput. Geotech.*, **104**, 237-246. https://doi.org/10.1016/j.compgeo.2018.08.021.
Zhang, L., Silva, F. and Grismala, R. (2005), "Ultimate lateral resistance to piles in cohesionless soils", *J. Geotech. Geoenviron. Eng.*, **131**(1), 78-83. https://doi.org/10.1061/(ASCE)1090-0241(2005)131:1(78).
Zhang, L.M. (2003), "Behavior of laterally loaded large-section barrettes", *J. Geotech. Geoenviron. Eng.*, **129**(7), 639-648. https://doi.org/10.1061/(ASCE)1090-0241(2003)129:7(639).
Zhou, H., Liu, H. and Kong, G. (2014), "Elastic analysis of a pile rectangular cross section under lateral load", *Soil Mech. Found. Eng.*, **51**(3), 126-131. https://doi.org/10.1007/s11204-014-9265-9.
Zhu, B., Li, T., Xiong, G. and Liu, J. C. (2016), "Centrifuge model tests on laterally loaded piles in sand", *Int. J. Phys. Model Geotech.*, **16**(4), 160-172. https://doi.org/10.1680/jphmg.15.00023.

*GC*